Published in final edited form as:
Phys Med Biol. 2009 November 21; 54(22): 6757–6771. doi:10.1088/0031-9155/54/22/001.

Cerenkov radiation imaging as a method for quantitative measurements of beta particles in a microfluidic chip

Jennifer S Cho, **Richard Taschereau**, **Sebastian Olma**, **Kan Liu**, **Yi-Chun Chen**, **Clifton K-F Shen**, **R Michael van Dam**, and **Arion F. Chatziioannou**
Crump Institute for Molecular Imaging, the Department of Medical and Molecular Pharmacology, David Geffen School of Medicine at UCLA

Abstract

It has been observed that microfluidic chips used for synthesizing ^{18}F-labeled compounds demonstrate visible light emission without nearby scintillators or fluorescent materials. The origin of the light was investigated and found to be consistent with the emission characteristics from Cerenkov radiation. Since ^{18}F decays through the emission of high-energy positrons, the energy threshold for beta particles, i.e., electrons or positrons, to generate Cerenkov radiation was calculated for water and polydimethylsiloxane (PDMS), the most commonly used polymer-based material for microfluidic chips. Beta particles emitted from ^{18}F have a continuous energy spectrum, with a maximum energy that exceeds this energy threshold for both water and PDMS. In addition, the spectral characteristics of the emitted light from ^{18}F in distilled water were also measured, yielding a broad distribution from 300 nm to 700 nm, with higher intensity at shorter wavelengths. A photograph of the ^{18}F solution showed a bluish-white light emitted from the solution, further suggesting Cerenkov radiation.

In this study, the feasibility of using this Cerenkov light emission as a method for quantitative measurements of the radioactivity within the microfluidic chip in situ was evaluated. A detector previously developed for imaging microfluidic platforms was used. The detector consisted of a charge coupled device (CCD) optically coupled to a lens. The system spatial resolution, minimum detectable activity and dynamic range were evaluated. In addition, a calibration of Cerenkov signal versus activity concentration in the microfluidic chip was determined. This novel method of Cerenkov radiation measurements will provide researchers with a simple yet robust quantitative imaging tool for microfluidic applications utilizing beta particles.

1. Introduction

Microfluidics is an emerging technology that facilitates the study of molecular processes in nano-liter levels in a finely controlled manner. The technology uses a network of channels and wells that are etched onto glass or polymer substrates to control the fluids inside. Many benefits can be achieved by using microfluidic chips due to the small amount of reagent required: high reaction efficiency, low cost, and flexibility in experiments. Along with these advantages, the technology also offers improved performance, such as high chemical yield and purity, and process integration.

Microfluidic chips have been designed for a multitude of applications, such as chemical synthesis, cell manipulation, DNA analysis, protein analysis, etc. (Andersson and van den Berg 2003, Sia and Whitesides 2003). One of the research interests is the development of a versatile,

jscho@mednet.ucla.edu

modular and automated microfluidic platform capable of synthesizing ^{18}F-labeled small molecules for Positron Emission Tomography (PET) imaging on demand (van Dam *et al* 2007, Whitesides 2006). It has been recently demonstrated that [^{18}F]fluoro-deoxy-glucose ([^{18}F]FDG), by far the most commonly used PET imaging tracer, can be successfully synthesized in a microfluidic platform. Using this microfluidic device, high radiochemical yield and purity were achieved with shorter synthesis time and far less cost compared to conventional automated synthesis (Lee *et al* 2005). Some collaborating research groups are thus developing novel probe synthesis methodologies by miniaturizing all the processes taken in large-scale conventional systems into coin-sized microfluidic chips (Olma *et al* 2008). With these microfluidic chips, each individual lab will be able to produce on-demand, the amount of PET imaging tracers customized for their own specific applications.

Although there is active research in the development of microfluidic devices for radiochemical synthesis of PET imaging tracers, not many tools are yet available for monitoring and analyzing the microfluidic chip and its development. Applying microfluidic systems to radiochemical synthesis is still in its nascent stage and one of the obstacles hindering the development of microfluidic chips is the lack of dedicated imaging systems. The process of chip design and manufacturing is iterative, and chip functionality test and failure analysis are crucial. Typically this information is gleaned from characterization of the chip output solution via traditional radioanalytical techniques, including thin layer chromatography (radio-TLC) and high performance liquid chromatography (radio-HPLC). In addition, the radioactivity of this chip output solution can be measured using a well-type gamma counter or a dose calibrator and compared with the input solution. These data though can be very difficult to interpret because they do not provide detailed information about unexpected losses of radioactivity. Losses can occur due to adsorption or absorption of ^{18}F-containing compounds, fluid trapped in dead volumes, or leaks caused by valve or chip defects that may arise during fabrication or due to harmful effects of chemicals and solvents on chip materials. The easiest way to find such points of failure in a chip during the radiochemical synthesis would be taking an image of the radioactivity distribution in-situ.

However, current methods of chip examination do not provide spatial information of the radioactivity distribution or the exact location of chip failure, leading to additional trial and error adjustments. In other words, current methods do not have imaging capability. Therefore, an imaging system that can pinpoint the exact location of failure in a microfluidic chip during radiochemical synthesis and quantify the 2D distribution of radiolabeled molecules, will provide researchers with a valuable tool to help design and develop many types of microfluidic chips. In addition, it will also serve as a monitoring and quality control tool for PET imaging probe production once the microfluidic platform is in use.

To image the spatial distribution of PET probes in a relatively large scale, scintillator-based systems such as preclinical imaging systems could be used. These systems, however, are not suitable for imaging microfluidic chips due to their high cost and limited availability. In addition, despite their adequate level of sensitivity, they do not have the spatial resolution capabilities to discern sub-millimeter structures of microfluidic chips. A dedicated imaging system for microfluidic chips should be compact and economical since the object to be imaged is the size of a coin and inexpensive to fabricate. Furthermore, the system requires high spatial resolution and adequate sensitivity as the microfluidic chip can contain a very small amount of activity.

PET tracers emit high-energy positrons that travel very short distances in matter before annihilation. Therefore, detection of these positrons can be directly used to map out the radioactivity distribution in a microfluidic chip during the imaging tracer synthesis process. Among radioisotopes which decay through the emission of *beta particles*, i.e., positrons or

electrons, there are many isotopes which are biocompatible, e.g. ^{3}H, ^{11}C, ^{14}C, ^{18}F, ^{32}P, etc. Due to the wide availability of these beta-emitting biocompatible isotopes, many studies have been conducted in the development of charged-particle (beta particle) imaging devices. Some devices were developed for imaging radioactivity distribution in tissue sections and have been commercialized (Cabello *et al* 2007, Kvinnsland *et al* 2002, Breskin 2000). Some were developed for intra-operative beta particle detection to assist in tumor localization during clinical surgery (Daghighian *et al* 1994, Raylmann 2000, Bogalhas *et al* 2008). However, few devices were optimized for microfluidic chip imaging (Cho *et al* 2006, 2007, Vu *et al* 2006, 2007, Laven *et al* 2004, 2005). In addition, most previously reported devices detect radiation either directly, through detection of the beta particles, or indirectly through scintillation light produced by the beta particles.

In this study, we propose a novel method for quantitative imaging of beta particles in a microfluidic chip in situ, by utilizing visible light emission from *Cerenkov radiation*. Cerenkov radiation is generated when a charged particle travels through an optically transparent material with a velocity greater than the speed of light in the medium. It has been observed that microfluidic chips used for ^{18}F-related radiochemical synthesis studies have shown unidentified visible light emission without nearby scintillators or fluorescent materials (figure 1). In this study, the origin of the light was investigated and its feasibility as a quantitative imaging source was evaluated.

2. Materials and methods

2.1. Cerenkov radiation validation

2.1.1. Cerenkov radiation energy threshold—Cerenkov radiation is produced by charged particles that travel through an optically transparent medium when the following condition is met:

$$\frac{1}{\beta n}<1 \tag{1}$$

where n is the refractive index of the medium and β is the ratio of the velocity of the particle in the medium to that of light in a vacuum ($\beta = v_p/c$). For a medium of given refractive index n, this relation determines the minimum charged-particle velocity required for Cerenkov radiation to occur, $\beta_{min}=(1/n)$. The parameter β is determined by the particle velocity, which is in turn related to the particle kinetic energy as follows (Knoll 2000, Jelley 1958):

$$E_{kinetic}=E_{total}-E_{restmass}=m_0c^2\left[\frac{1}{\sqrt{1-\beta^2}}-1\right] \tag{2}$$

where m_0c^2 represents the rest-mass energy of the particle. Since ^{18}F decays through the emission of high-energy positrons, based on (1) and (2), the minimum particle kinetic energy, E_{thresh}, for beta particles to generate Cerenkov radiation was calculated for water and polydimethylsiloxane (PDMS), and compared to the energy spectrum of positrons emitted from ^{18}F. These two materials were chosen, since they are the most commonly encountered materials in microfluidics.

2.1.2. Cerenkov radiation emission spectrum—The spectral characteristics of the emitted light from the ^{18}F-containing solution in distilled water (^{18}F in $[^{18}O]H_2O$) were measured using a spectrofluorometer (FluoroMax-3, Horiba Jobin Yvon, NJ). A solution

containing a total of 11 mCi of ^{18}F was placed in a syringe. With the spectrofluorometer excitation source turned off, the light signal from the syringe was acquired over a wavelength range of 200 nm to 1000 nm, at 10 nm intervals with 10 nm widths, for 1 second per interval. The relatively high radioactivity (~11 mCi) resulted in a significant increase in background counts in the measured data due to direct interactions of 511-keV gamma rays with the photomultiplier tube (PMT) photocathode inside the spectrofluorometer. Therefore, background counts from two different sources were measured separately: first, the PMT thermionic emission dark counts and second, the background counts from 511-keV gamma rays. The PMT dark counts were measured with the detector shutter closed and no radiation placed inside or nearby. The background counts from 511-keV gamma rays were measured with an ^{18}F solution of known radioactivity placed in the measurement chamber and the detector shutter covered with black tape, allowing only 511-keV gamma rays to penetrate, while blocking any visible light. This measurement resulted in background counts from both the PMT dark counts and 511-keV gammas. The PMT dark counts were then subtracted from the total background in order to calculate the background counts only from 511-keV gammas so that decay correction could be applied to the measured spectrum. In the measured Cerenkov radiation emission spectrum, corrections were applied for detector dark current and ^{18}F radioactive decay, as well as the background counts from 511-keV gamma rays.

This background and decay corrected data was further corrected for both the PMT photocathode quantum efficiency and the water-filled syringe transmittance in order to calculate the original Cerenkov radiation emission spectrum inside a syringe. The PMT quantum efficiency was provided by the manufacturer and the transmittance of the water-filled syringe was measured using a spectrophotometer (Ultrospec 1100 pro, GE Healthcare, NJ) from 200 nm to 900 nm at 20 nm intervals. All the measurements were repeated 10 times and averaged. The error bars for each data point were calculated to include Poisson noise propagation from all the corrections.

2.2. Microfluidic chips

The microfluidic chips used in our study were made from PDMS. A typical microfluidic chip cross section is shown in figure 2. It usually consists of three layers: a fluidic layer (A-layer), a control layer (B-layer) and a substrate layer (C-layer). Fluids of interest, for example ^{18}F solution and other chemicals pertinent to radiochemical synthesis, are placed in a fluidic channel and their movement is usually controlled by pressure-actuated valves manipulated by microchannels on the control layer (Unger *et al* 2000). However, the microfluidic chip used in our study only consisted of two layers, a fluidic layer and a substrate layer with no intervening control layer in between. That was in order to simplify the chip geometry without sacrificing the fundamental chip properties for the measurements. In this study, the relevant chip properties to Cerenkov radiation emission were the refractive index of the microfluidic chip material and the size of the fluidic channel. Therefore, using microfluidic chips with two layers, instead of three layers, would not make any difference in measurements as long as the layers were made from the same materials in this case PDMS, and thick enough to stop all beta particles inside.

2.3. Microfluidic chip (PDMS) optical transmittance

Since Cerenkov radiation produces visible light, optical transmittance of the microfluidic material plays an important role in the overall system sensitivity. Therefore, the transmittance of PDMS from two manufacturers, GE and Sylgard, was measured using a spectrophotometer (8453, Agilent Technologies, CA), for light wavelengths ranging from 200 to 1100 nm. From GE, the PDMS was made by the RTV 615 elastomer kit (components A:B mixed in 10:1 ratio) and cured by baking at 80°C for 4 hours. From Dow-Corning, the PDMS was made by the Sylgard 184 elastomer kit (components A:B mixed in 10:1 ratio) and cured by baking at 80°C for 4 hours.

2.4. Lens-coupled CCD detector

A schematic diagram of the lens-coupled charge-coupled device (CCD) detector is presented in figure 3. The camera was an SBIG ST-2000XM (SBIG, Santa Barbara, CA) and employed a Kodak KAI-2020M interline-transfer CCD sensor. The CCD sensor had 1600 × 1200 pixels with a pixel pitch of 7.4 μm. The CCD sensor temperature was regulated at −15°C with a Peltier thermoelectric device aided with a water cooling system. A C-mount lens (EL1025B 0.95/25, Universe Kogaku America, NY) with a focal length of 25 mm was mounted. The lens aperture was set to be 0.95, the largest, to maximize light collection efficiency.

The microfluidic chips to be imaged were placed on a motorized stage (RCF-mini1, Jim's Mobile, Inc., Lakewood, CO) with the fluidic channel side up, and the entire setup was placed inside a light-tight box. The motorized stage was used to remotely control the vertical position of the microfluidic chip with respect to the lens for focusing. It was controlled by a USB controller (FCUSB, Shoestring Astronomy, IA) connected through the light-tight box to the computer. This allowed remote controlled operation and reduced radiation exposure to users by keeping them at a distance from the radioactivity within the chip during the focusing process.

The lens-to-object distance was 5.7 cm and the full field-of-view was 4 cm × 3 cm with an image-to-object magnification of 0.3. Using a pixel binning of 3×3, this setup yielded a sampling pitch of 74 μm in the object plane.

2.5. Image processing and background investigation

2.5.1. Cerenkov radiation image processing—All Cerenkov radiation images acquired from the system were corrected for three factors: CCD dark current, lens vignetting and 511-keV gamma rays. The master dark frame was obtained by averaging 100 dark-current images acquired for 5 minutes each at −15°C. This master dark frame was subtracted from the raw image immediately after each acquisition to correct for CCD thermal noise.

A flat field correction to compensate for lens vignetting was then applied by dividing the dark-current corrected image by a master flat field image. The master flat field image was obtained by averaging 100 uniformly illuminated bright field images and then dividing it by the mean pixel value. The flat field correction allowed the system to reliably reproduce the Cerenkov radiation signal proportional to radioactivity on the entire field.

When radioactivity was present in a microfluidic chip, some 511-keV gamma rays directly interacted with the CCD sensor depositing significant amount of energy and subsequently left speckle noise on the image. This noise manifested randomly distributed white pixels with very large pixel values which could interfere with the quantification of the image signals from Cerenkov radiation. Therefore, a 3×3 median filter was applied to the image in order to remove the speckle noise from the 511-keV gamma rays. These three corrections enabled the Cerenkov radiation images to be physically meaningful and quantitatively accurate for further analysis.

2.5.2. 511-keV gamma ray background—Further investigation was conducted on the relationship between the amount of speckle noise from 511-keV gamma rays as a function of a total radioactivity inside a chip. In order to accurately measure the amount of speckle noise from the 511-keV gamma rays, two other sources of speckle noise were subtracted: the CCD inherent hot pixels and cosmic rays. The CCD inherent hot pixels were the defective pixels which always generated higher pixel values in the same positions. Therefore, these could be corrected via the master dark frame subtraction process. The amount of speckle noise from the direct interaction of cosmic rays with the CCD sensor was then measured as follows. From each of 100 dark current images, the master dark frame was subtracted to only leave the randomly scattered white pixels from cosmic rays while subtracting the CCD inherent hot

pixels. Then the number of white pixels in each of 100 images was averaged to obtain the average cosmic ray interaction with the CCD sensor. The number of speckle noise from cosmic rays was consequently subtracted from the total number of speckle noise in the image to get the exact amount of speckle noise from 511-keV gamma rays.

2.6. Cerenkov radiation spatial resolution

2.6.1. Line-pair microfluidic chip—The system spatial resolution was measured with a custom designed line-pair microfluidic chip. The chip consisted of a snaked line channel with a 200-μm width, a 33-μm depth and a 300-μ space between the channels edge-to-edge (figure 7). The channel was filled with 20 μCi of [^{18}F]FDG solution ([^{18}F]FDG in [^{18}O]H_2O) and imaged for 5 minutes. The [^{18}F]FDG solution was used because it was readily available from the in-house cyclotron facility. Chemically, an [^{18}F]FDG solution is different from a [^{18}F] fluoride solution. But physically, and from a nuclear-decay perspective, both will emit positrons in exactly the same manner.

2.6.2. FWHM and MTF—The system spatial resolution was investigated in more detail by measuring the full width at half maximum (FWHM) of the line profile of a microchannel. A microfluidic chip consisted of a line channel with a width of 200 μm, a depth of 30 μm, and a length of 13 mm (figure 8). The channel was filled with [^{18}F]FDG solution having an activity concentration of 107 μCi/μL and imaged for 5 minutes. The activity concentration was calibrated by measuring the total activity and the weight of the [^{18}F]FDG solution contained in the chip, using a dose calibrator and a high-precision scale. The weight of the solution was converted to the volume using the known density of water. Since the concentration of [^{18}F] FDG was extremely low (< nM concentration), we assumed that it had negligible effect on the solution density. The line profile of the channel was acquired and the FWHM and the corresponding modulation transfer function (MTF) were calculated.

2.7. Cerenkov radiation signal calibration curve

A signal calibration curve, which describes the light output from Cerenkov radiation as a function of radioactivity concentration was obtained. The microfluidic chip was made from PDMS, which had a refractive index of 1.41 (Kocabas *et al* 2006). The chip consisted of microchannels with a length of 7 mm, width of 1 mm and a depth of 125 μm (figure 4). The PDMS substrate layer of the chip was intentionally made thicker (~3 mm) than usual (~50 μm) in order to ensure that all beta particles interact within the PDMS chip and not in the underlying glass slide. A microchannel was filled with 30 μCi of [^{18}F]FDG solution (~30 μCi/μL or ~1110 MBq/cc including the inlet and the outlet volume) and an additional slab of PDMS layer was placed on top, to prevent water evaporation from the inlet and the outlet during the overnight measurement. The total light signal was measured for 5 minutes at 10-minute intervals during the radioactive decay. In the calibration curve, the slope of the curve was divided by the acquisition time (5 min.), in order to get the signal rate from Cerenkov radiation in PDMS.

2.8. MDA and dynamic range

The minimum detectable activity (MDA) specifies the lowest amount of radioactivity that can be *reliably* measured by a system. The MDA is determined by the system noise level to ensure that both the false positive and false negative probabilities of determining the presence of radiation were less than 5% (Currie 1968). The MDA of our system with the Cerenkov radiation signal from PDMS was measured using the same microfluidic chip used for the signal calibration. The microchannel was filled with an [^{18}F]FDG solution and a 1 mm × 1 mm region of interest (ROI) was drawn inside the uniform activity region on the Cerenkov signal image. The average pixel value in the ROI was measured as a function of radioactivity concentration

per unit area ($\mu Ci/mm^2$) for 5-minute exposures with 10-minute intervals as the ^{18}F decayed. When the mean signal crossed the MDA level predetermined by the system background, the corresponding radioactivity concentration was measured.

The system dynamic range was also calculated by comparing the mean pixel value in the ROI to the pixel full well capacity. The maximum detectable activity was determined when the average pixel signal met the full well of the 16-bit CCD pixel.

3. Results

3.1. Cerenkov radiation validation

3.1.1. Cerenkov radiation energy threshold—Table 1 lists the calculated energy threshold, E_{thresh}, for a beta particle to generate Cerenkov radiation in water and PDMS. The threshold energy is inversely related to the refractive index of the material (Knoll 2000,Jelley 1958). This means that more light will be produced from Cerenkov radiation in a material with a higher refractive index. Compared to the energy spectrum of positrons emitted from ^{18}F, which has a maximum energy of 633 keV and an average energy of 250 keV (Cherry *et al* 2003), the maximum energy of positrons from ^{18}F exceeded the energy threshold in both water and PDMS. Thus, beta particles (positrons) from ^{18}F with energies higher than the energy threshold will generate Cerenkov radiation in both water-based ^{18}F solution and a microfluidic chip made from PDMS.

3.1.2. Cerenkov radiation emission spectrum—The PMT dark counts were measured to be 750 counts/sec (cps) at room temperature, whereas the background counts from 511-keV gamma rays were measured to be approximately 100 cps/mCi, resulting in 1100 cps with 11 mCi of ^{18}F in our measurements. After the background and decay corrections, the measured spectrum of the emitted light from the ^{18}F-containing solution showed a broad and continuous distribution from 300 nm to 700 nm shown as the lower, empty-square line in figure 5. Unlike typical scintillation light which manifests a relatively narrow emission spectrum, this broad spectrum suggested that the origin of the light could be Cerenkov radiation (Knoll 2000,Jelley 1958). It is worth noting that the UV absorption of a plastic syringe caused the minimum wavelength cutoff at 280 nm.

After the PMT quantum efficiency and the syringe transmittance corrections, the spectrum was consistent with the theoretical Cerenkov emission spectrum (dotted line) from 300 nm to 580 nm, inversely proportional to the square of the wavelength (solid square in figure 5) (Jelley 1958). Above 600 nm, however, the PMT quantum efficiency was very low and this resulted in a deviation of the measured spectrum from the theoretical emission curve. The error bars clearly show that the measured data could have large possible errors introduced and further amplified due to the correction of the low PMT quantum efficiency. Therefore, further investigation and more carefully controlled measurements are required in longer wavelengths.

3.2. Microfluidic chip (PDMS) optical transmittance

The optical transmittance of PDMS as a function of wavelength is shown in figure 6. The PDMS from both manufacturers showed similar transmittance properties. Above 400 nm, more than 90% of the light was transmitted.

3.3 Image processing and background investigation

The median filtering effectively removed the speckle noise from high-energy gamma rays and cosmic rays while conserving the image signals generated from low-energy visible light of Cerenkov radiation.

The level of speckle noise from cosmic rays was measured to be 11 counts for 5 minute acquisitions, which was equivalent to 2 counts/min/cm^2. After subtracting this number from the amount of speckle noise on the acquired images, it was shown that the remaining speckle noise was proportional to the total radioactivity inside a chip. Only 0.00009% of the total 511-keV gamma rays emitted during the acquisition actually interacted with the CCD sensor in the current camera setup, which was equivalent to 2 gammas/μCi/min on the image.

3.4. Cerenkov radiation spatial resolution

As shown in figure 7, the line pairs with a 200-μm width and a 300-μm spacing edge-to-edge were discernable with a visual assessment of the Cerenkov signal image. In addition, the line profile of the microchannel was acquired and the FWHM was measured to be 350 μm (figure 8). This resolution was dominated by the physical size of the channel, which was 200 μm. The corresponding MTF calculated from the line profile is shown in figure 9 and gives 2.24 mm^{-1} at 10% of MTF. This final MTF was a convolution of the channel width of 200 μm, positron range, Cerenkov radiation MTF, lens MTF, and CCD sensor MTF. Disregarding the physical size of the channel, the Cerenkov image spatial resolution was largely limited by the positron range. There have been many studies about the range of charged particles, and the FWHM of the distribution of the positron annihilation end point of ^{18}F in x-coordinates was claimed to be greater than 100 μm in water (Levin and Hoffman 1999).

3.5. Cerenkov radiation signal calibration curve

The signal calibration curve of Cerenkov radiation from PDMS is shown in figure 10 in a log-log scale with the activity concentration in reverse order (x-axis) to better visualize the ^{18}F decay over time. The observed linearity of the measured signal versus activity concentration makes quantitative imaging possible. The Cerenkov signal rate for PDMS (n=1.41) was measured to be 0.047 ADU/nCi/sec, where ADU stands for analog-to-digital unit in the CCD camera. This final signal rate is a combination of the Cerenkov light output, the PDMS optical transmittance, the system lens coupling efficiency (Liu *et al* 1994, Yu 1997), the CCD quantum efficiency and the CCD readout amplifier gain. However, it should be noted that this signal rate is purely from PDMS and not from the underlying glass slide. The substrate layer of the chip was intentionally made thick so that all the beta particles stop inside the PDMS. Therefore, with typical chip geometry that has a glass slide underneath a thin substrate PDMS layer (50~100 μm) to provide mechanical rigidity, the Cerenkov light output will increase due to higher refractive index of glass, resulting in higher signal rate and higher system sensitivity. Given the linearity of the calibration that we have observed, it should be straightforward to generate a calibration curve for different thicknesses and materials in the microfluidic layers. Alternatively, due to the low cost of manufacturing of the microfluidic chips, one could perform a calibration measurement with a similar chip.

3.6. MDA and dynamic range

The system MDA was measured to be 0.19 μCi/mm^2 for 5-minute acquisitions (figure 10) and the maximum detectable activity was calculated to be 741.54 μCi/mm^2 for 5-minute acquisitions. This provides more than three orders of magnitude of dynamic range. However, the upper end of the dynamic range can be very easily improved by using a shorter camera acquisition time and a smaller lens aperture setting. In addition, the measured MDA is chip-geometry dependent and therefore could vary depending on the specific microfluidic chip used.

The Cerenkov radiation signal from the microfluidic chips in our study was in fact from two different materials: PDMS and water. High-energy positrons can travel a certain distance in matter before they annihilate and will generate Cerenkov radiation as they lose their energy along the path from the aqueous solution to the PDMS. Due to the difference in the refractive indices of water and PDMS (1.33 and 1.41, respectively), each beta particle will produce

slightly different amounts of Cerenkov radiation depending on whatever path they travel in a chip. In this study, however, the Cerenkov light output from water and PDMS was assumed to be the same and this will cause some discrepancy when using different microfluidic chip geometries.

In addition, throughout the measurements, the depth of the microchannels was not controlled and varied from 30 μm to 125 μm. This is because the microfluidic chips used in our measurements were selected from samples readily available in-house that were designed for different applications, and this could eventually affect the system performance, especially in MDA. For example, the MDA will likely be worse for a chip with a thicker fluidic channel, containing water, than with a thinner channel because of the lower refractive index of water compared to that of PDMS. The MDA will probably be better for a chip with thinner control and substrate layers because more beta particles will likely interact with an underlying glass slide which has a higher refractive index (n=1.5) than PDMS or water. Therefore, the chip geometry should be controlled in the future and the effect of different chip geometries on the system performance needs to be further investigated.

Lastly, it is worth noting that other radionuclides that emit beta particles with higher maximum energies (e.g., ^{32}P emits electrons with a maximum energy of 1.71 MeV.) will produce more light from Cerenkov radiation, resulting in better MDA, yet poorer spatial resolution.

4. Conclusions

This work has demonstrated that beta particles emitted from ^{18}F in a microfluidic chip generate visible light emission that is consistent with the characteristics of Cerenkov radiation, and this signal can be detected using a lens-coupled CCD system developed for imaging microfluidic chips. The feasibility of utilizing this light emission as a quantitative imaging source was evaluated by measuring the spatial resolution, signal calibration curve, minimum detectable activity and dynamic range of the prototype system.

This technology is already being used at our institute to troubleshoot microfluidic chip development. Figure 1 shows an example where this method is currently used. This study investigates the effect of adsorption of ^{18}F-labeled molecules from an aqueous solution to PDMS as it advances through a mixing channel. As shown in the figure, the ^{18}F-labeled compound was adsorbed on the surface of the channel and gradually diminished as the solution became depleted.

The merit of this technology lies in its simplicity. This method allows for a standard microfluidic chip to be used with no major modification for beta particle imaging. Furthermore, a room light photograph of the chip can be acquired with the same camera setup used for activity measurements and overlaid with a Cerenkov image, so that they can together provide the structural information of the chip, as well as the radioactivity distribution. The relatively low sensitivity compared to scintillation technology could be a drawback of this technology.

Preliminary measurements in light output and sensitivity using Cerenkov radiation versus the scintillation technology showed that the light output of Cerenkov radiation is less than 1% of that of plastic scintillator (BC-400, Saint-Gobain Crystals, OH). This is consistent with measurements that exist in the literature (Ross 1969). However, some applications require relatively high levels of radioactivity in a chip, which will compensate for the low sensitivity of the Cerenkov radiation method. For example, microfluidic chips developed for radiochemical synthesis of PET imaging probes usually require *at least* 100 μCi of ^{18}F solution for small animal imaging per mouse and 10 mCi for clinical PET scans per patient in total injected in a chip (Lee *et al* 2005). This is approximately equivalent to activity concentration of 20 μCi/mm^2 and 500 μCi/mm^2, respectively, depending on microfluidic chip geometry,

which is significantly above the system MDA measured with Cerenkov radiation. Therefore, the relatively low sensitivity of Cerenkov radiation should not place any limitation on imaging in these applications.

In conclusion, this novel imaging technology using Cerenkov radiation will provide a simple yet robust quantitative imaging tool for microfluidic applications utilizing charged particles. It will be of benefit to researchers by providing a tool to further investigate and develop microfluidics for radiochemical synthesis (e.g. design, material surface adsorption measurements, etc.) as well as a method for routine imaging in synthesis environment (e.g. to get quantitative measurements of yield of various radiochemical steps). In addition, it might also serve as a quality control tool for the PET imaging probe production once this microfluidic platform is in use. As such, the technology will be of great interest to both developers of novel microfluidic chips as well as to users of these microfluidic devices.

Acknowledgments

The authors would like to thank the Crump Institute for Molecular Imaging preclinical imaging facility staff members, Dr. David Stout, Robert Silverman, Waldemar Ladno, Judy Edwards and Benjamin Chun for their help with the radioactivity work, and Drs. Nam Vu, Ali Douraghy and Qinan Bao for their valuable discussions. This study was supported by the National Institutes of Health under Grant No R24 CA92865 and the Department of Energy under Contract No DE-FC03-02ER63420.

References

Andersson H, van den Berg A. Microfluidic devices for cellomics: a review. Sensors and Actuators B: Chemical 2003;92:315–325.

Bogalhas F, Menard L, Bonzom S, Palfi S, Siebert R, Duval M, Lefebvre F, Pinot L, Pitre S, Charon Y. Physical performance of an intraoperative beta probe dedicated to glioma radioguided surgery. IEEE Transactions on Nuclear Science 2008;55(no 3):833–841.

Breskin A. Advances in gas avalanche radiation detectors for biomedical applications. Nucl. Instr. Meth January;2000 A454:26–39.2000

Cabello J, Bailey A, Kitchen I, Prydderch M, Clark A, Turchetta R, Wells K. Digital autoradiography using room temperature CCD and CMOS imaging technology. Phys. Med. Biol 2007;52:4993–5011. [PubMed: 17671349]

Cherry, SR.; Sorenson, JA.; Phelps, ME. Physics in Nuclear Medicine. Saunders; Philadelphia: 2003.

Cho, JS.; Vu, NT.; Chung, YH.; Yu, ZT.; Silverman, RW.; Taschereau, R.; Tseng, HR.; Chatziioannou, AF. Detection of beta particles in a microfluidic chip using a scintillator and CCD; IEEE Nuclear Science Symp. and Medical Imaging Conf. record; San Diego, CA. 29 Oct. – 3 Nov. 2006; 2006. 2006

Cho, JS.; Vu, NT.; Yu, ZT.; Silverman, RW.; Taschereau, R.; Tseng, HR.; Chatziioannou, AF. Optimization of design parameters of a prototype CCD-based lens-coupled imaging system for the detection of beta particles in a microfluidic chip; IEEE Nuclear Science Symp. and Medical Imaging Conf. record; Honolulu, Hawaii. Oct. – 27 Nov. 3, 2007; 2007.

Currie LA. Limits for qualitative detection and quantitative determination. Anal. Chem 1968;40:586–593.

Daghighian F, Mazziotta JC, Hoffman EJ, Shenderov P, Eshanhian B, Siegel S, Phelps ME. Intraoperative beta probe: A device for detecting tissue labeled with positron or electron emitting isotopes during surgery. Med. Phys 1994;21(1):153–157. [PubMed: 8164582]

Jelley, JV. Cerenkov Radiation and its Applications. Pergamon Press; London: 1958. Chap.1–2

Knoll, GF. Radiation Detection and Measurement. John Wiley & Sons, Inc; Ney York: 2000. Chap. 19

Kocabas A, Ay F, Dana A, Aydinli A. An elastomeric grating coupler. J. Opt. A: Pure Appl. Opt 2006;8:85–87.

Kvinnsland Y, Bruland O, Moe L, Skretting A. A method for measurement of the uptake patterns of two beta-emitting radionuclides in the same tissue section with a digital silicon detector: application to a

study of 89SrCl2 and 153Sm-EDTMP in a dog with spontaneous osteosarcoma. Eur J Nucl Med Mol Imaging Feb;2002 29(2):191–7. [PubMed: 11926381]2002

Laven M, Wallenborg S, Velikyan I, Bergstrom S, Djodjic M, Ljung J, Berglund O, Edenwall N, Markides KE, Langstrom B. Radionuclide imaging of miniaturized chemical analysis systems. Anal. Chem 2004;76:7102–7108. [PubMed: 15571365]

Laven M, Velikyan I, Djodjic M, Ljung J, Berglund O, Markides K, Langstrom B, Wallenborg S. Imaging of peptide adsorption to microfluidic channels in a plstic compact disc using a positron emitting radionuclide. Lab Chip 2005;5:756–763. [PubMed: 15970969]

Lee CC, et al. Multistep synthesis of a radiolabeled imaging probe using integrated microfluidics. Science 2005;310(no 16):1793–1796. [PubMed: 16357255]

Levin CS, Hoffman EJ. Calculation of positron range and its effect on the fundamental limit of positron emission tomography system spatial resolution. Phys. Med. Biol 1999;44(1999):781–799. [PubMed: 10211810]

Liu H, Karellas A, Harris LJ, D'Orsi CJ. Methods to calculate the lens efficiency in optically coupled CCD x-ray imaging systems. Med. Phys July;1994 21(7):1193–1195. [PubMed: 7968853]1994

Olma, S.; Liu, K.; Chen, YC.; Tseng, HR.; van Dam, RM.; Shen, CK. the Proc. of μTAS. San Diego, CA: Oct 12-16. 2008 Application of a microfluidic droplet mixer for [^{18}F]flourine labeling of biomolecules for Positron Emission Tomography; p. 6042008

Raylmann RR. A solid-state intraoperative beta probe system. IEEE Transactions on Nuclear Science 2000;47(no 4):1696–1703.

Ross HH. Measurement of β-emitting nuclides using Cerenkov radiation. Anal. Chem 1969;41:1260–5.

Sia S, Whitetsides G. Microfluidic devices fabricated in poly(dimethylsiloxane) for biological studies. Electrophoresis 2003;24:3563–3576. [PubMed: 14613181]

Unger MA, Chou H-P, Thorsen T, Scherer A, Quake SR. Monolithic microfabricated valves and pumps by multilayer soft lithography. Science 2000;288(5463):113–116. [PubMed: 10753110]

van Dam, RM., et al. Proc. of NanoTech. Santa Clara, CA: 2007. Automated microfluidic-chip-based stand-alone instrument for the synthesis of radiopharmaceuticals on human-dose scales. May 20–24

Vu, NT.; Chung, YH.; Yu, ZT.; Silverman, RW.; Taschereau, R.; Farrell, R.; Shah, KS.; Tseng, HR.; Chatziioannou, AF. Direct detection of beta particles on a microfluidic chip using position sensitive APDs; IEEE Nuclear Science Symp. and Medical Imaging Conf. Record; San Diego, CA. 29 Oct. – 3 Nov. 2006; 2006.

Vu, NT.; Yu, ZT.; Silverman, RW.; Farrell, R.; Shah, KS.; Tseng, HR.; Chatziioannou, AF. Performance of an integrated microfluidic chip and position sensitive APD for the detection of beta emitting probes in cell cultures 2007; Nuclear Science Symp. and Medical Imaging Conf. Record; Honolulu, Hawaii. Oct. – 27 Nov. 3, 2007; 2007.

Whitesides GM. The origins and the future of microfluidics. Nature 2006;442:368–373. [PubMed: 16871203]

Yu T, Boone JM. Lens coupling efficiency: Derivation and application under differing geometrical assumptions. Med. Phys 1997;24(4):565–570. [PubMed: 9127309]

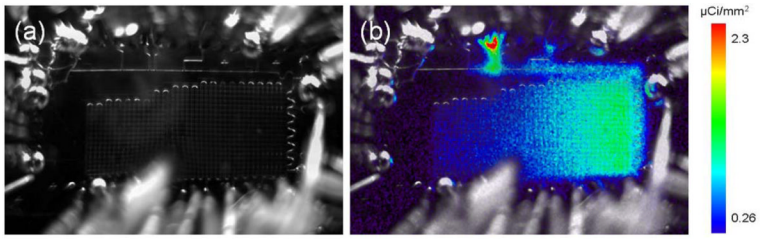

Figure 1.
(a) Room light photograph of a microfluidic chip containing ^{18}F-labeled compound residue in the microfluidic channels with a channel width of 200 μm. (b) Cerenkov signal image of the same microfluidic chip overlaid on the room light photograph (artificially colored).

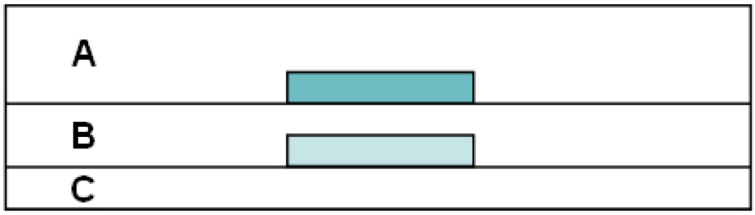

Figure 2.
A typical microfluidic chip cross section: (A) fluidic layer, (B) control layer and (C) substrate layer. The colored areas represent microchannels on the fluidic layer and the control layer, respectively. Fluids of interest are placed in a fluidic channel and their movement is controlled by pressure-actuated valves manipulated by microchannels on the control layer.

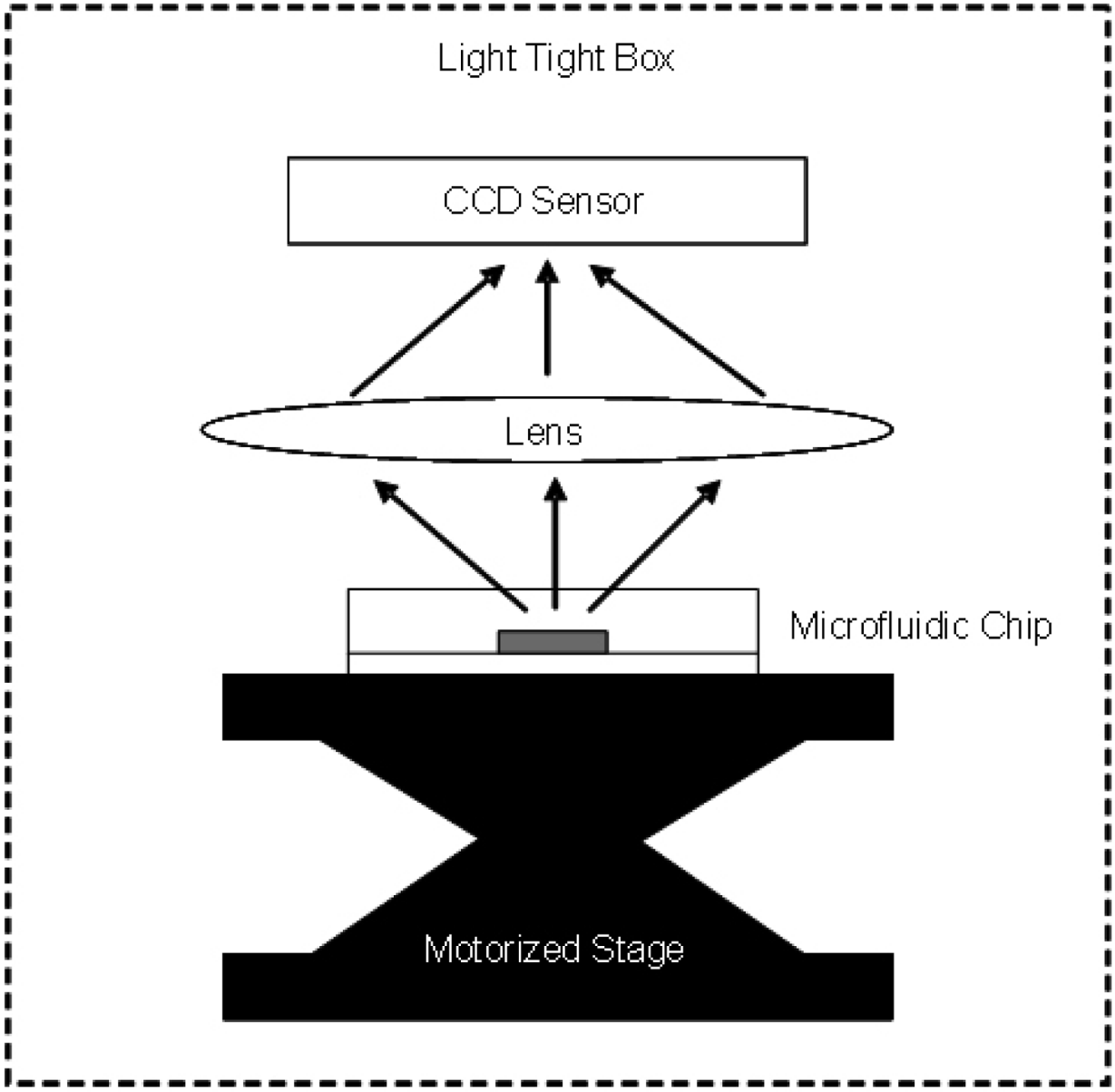

Figure 3.
Schematic figure of the lens-coupled CCD system.

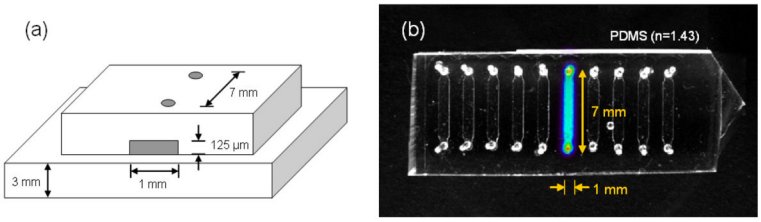

Figure 4.
(a) Microfluidic chip geometry used for the signal calibration. (b) A room light photograph of the chip, used for signal calibration measurement, overlaid with artificially-colored Cerenkov signals.

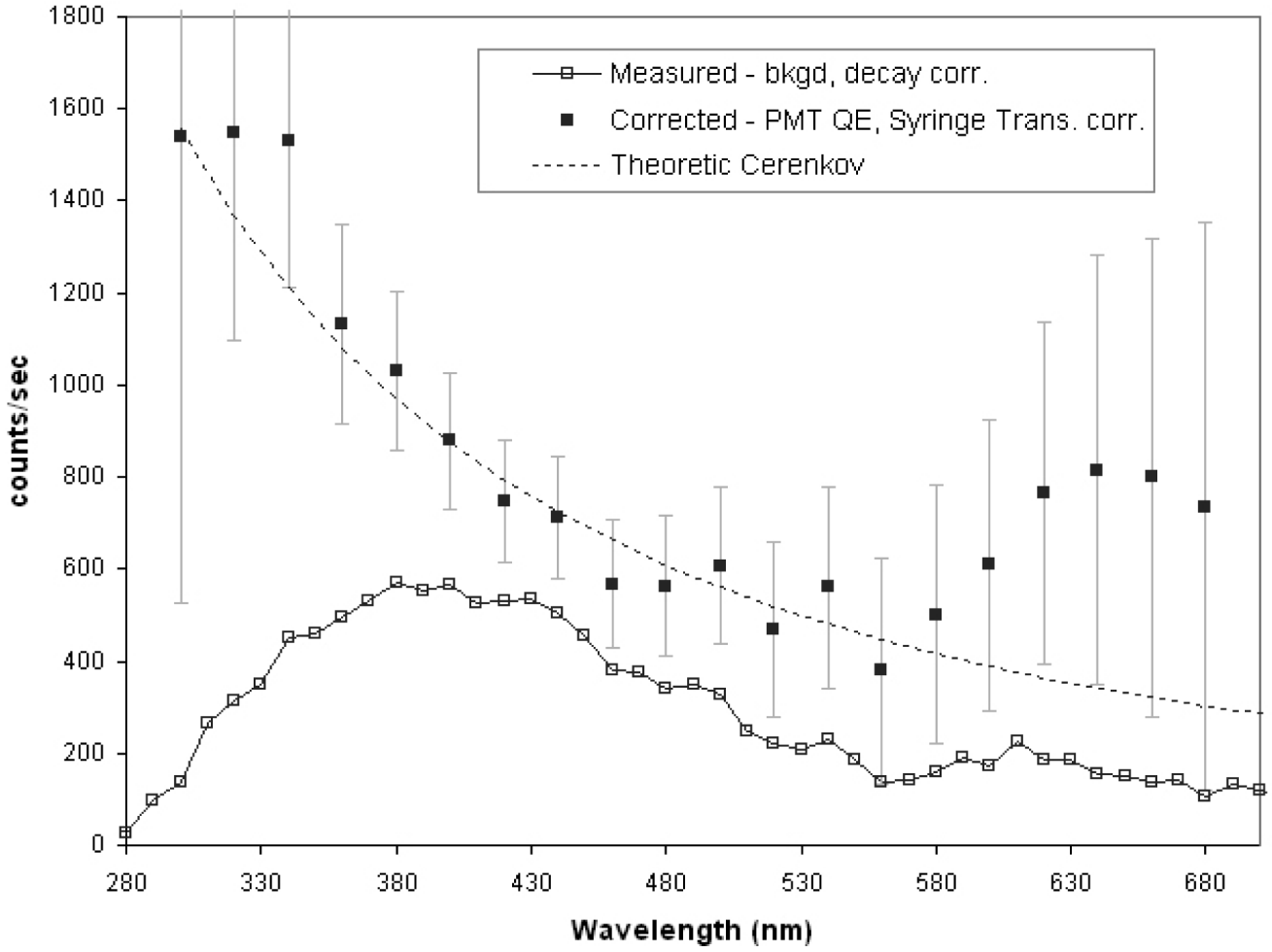

Figure 5.

Spectral characteristics of the emitted light from an aqueous ^{18}F solution. The measured spectrum showed a broad and continuous distribution with higher intensity at shorter wavelengths. After the PMT quantum efficiency and the syringe transmittance corrections, the spectrum followed the theoretical Cerenkov emission spectrum from 300 nm to 580 nm, inversely proportional to the square of the wavelength.

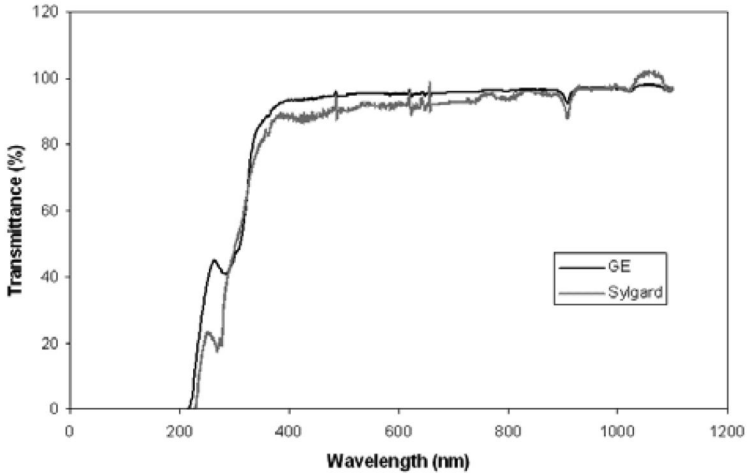

Figure 6.
Transmittance properties of PDMS from two manufacturers.

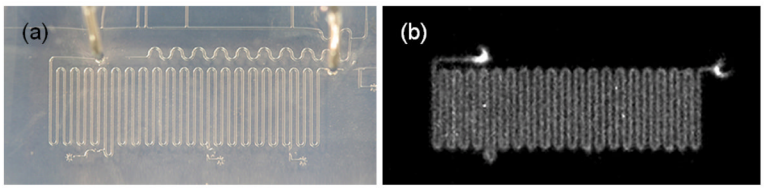

Figure 7.
Cerenkov radiation imaging spatial resolution measurement. (a) A room light photographic image of a line pair microfluidic chip. The chip consisted of line channels with a thickness of 200 μm, and a spacing of 300 μm edge-to-edge. (b) A Cerenkov radiation image of the chip filled with [^{18}F]FDG solution. The line pairs were clearly discernable.

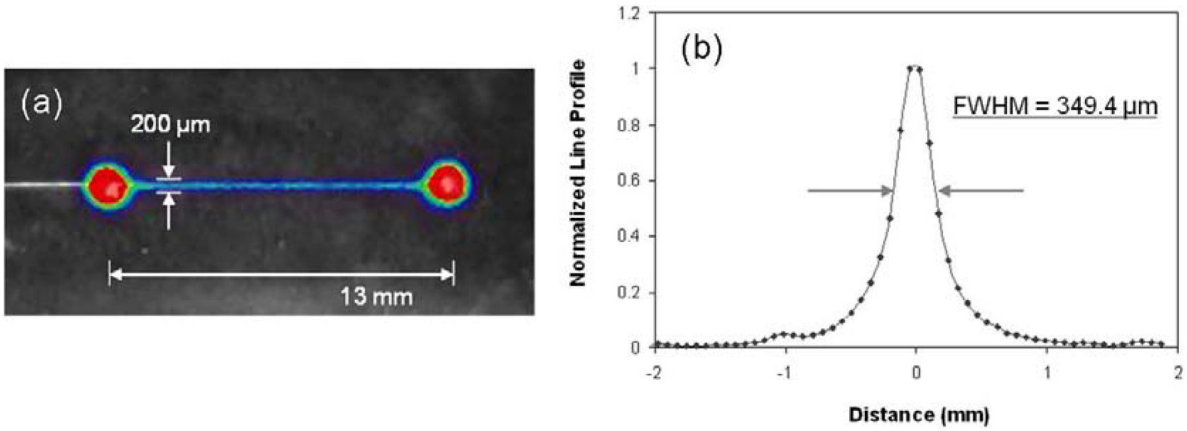

Figure 8.

Cerenkov radiation imaging spatial resolution measurement. (a) Artificially colored Cerenkov signal image overlaid on top of room light photograph of the line channel with a of 200 µm width. (b) A line profile of the microchannel. This resolution was dominated by the physical size of the channel.

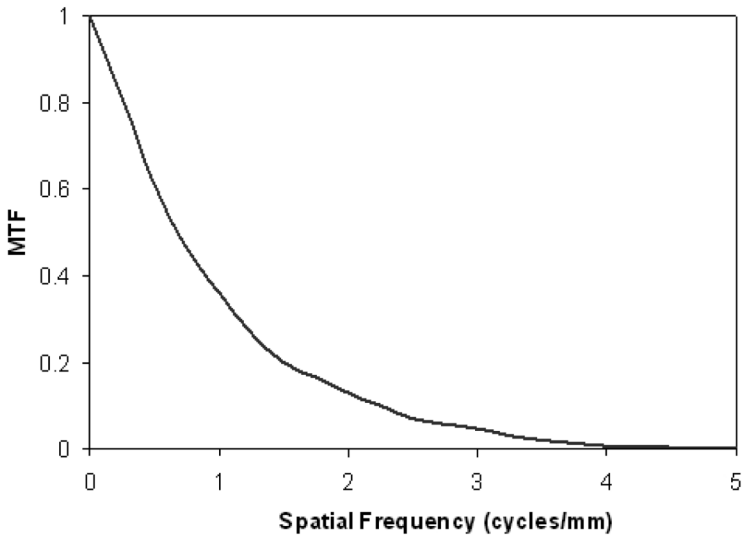

Figure 9.
The corresponding modulation transfer function (MTF) for the line profile of the channel from figure 8.

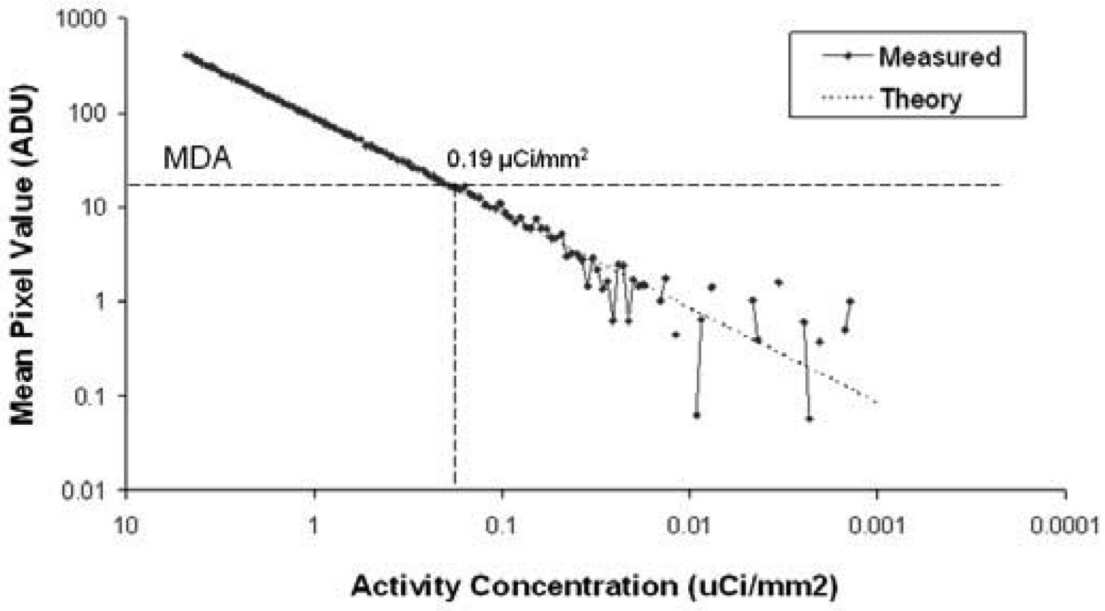

Figure 10.
The system linearity and minimum detectable activity measurements.

Table 1

Material refractive indices with corresponding minimum particle velocities and Cerenkov threshold energy.

	n	$\beta_{min} > 1/n$	E_{thresh} (keV)
water	1.33	0.752	264.06
PDMS	1.41	0.699	203.86